

two-dimensional models, the effective mass falls steeply as wavelength decreases. In three-dimensional models, in a fairly broad frequency range near the response peak, the effective mass becomes substantially less sensitive to wavelength<sup>14,15</sup>. In light of this behaviour, and the intuitive argument above, the observed lack of frequency sensitivity in the penetration depth does not seem all that surprising. □

**Methods**

**Pressure sensor**

A sensor consists of a glass capillary (inner and outer diameters 100 and 170 μm, respectively) tipped with a gold-coated polymer diaphragm. Light from an LED is delivered via a fibre optic threaded into the capillary, and reflects from the diaphragm. The amount of light returning to the fibre optic for transmission to a photodetector varies linearly with the pressure-induced bending of the diaphragm. The acoustic impedance of the sensors is an order of magnitude larger than that of the cochlea, and their presence does not 'load' the cochlea outright. Nevertheless, in some animals small reversible changes in compound action potential (CAP) threshold and/or scala vestibuli pressure occurred when the scala tympani sensor was close to the basilar membrane. However, the derived fluid velocity close to the basilar membrane was similar to that measured directly by others<sup>11,12</sup>, suggesting that the sensor's presence does not cause large changes in cochlear mechanics.

**Experimental procedure**

Animal procedures were approved by the Princeton University IACUC. The experimental animals were young adult gerbils. A gerbil was deeply anaesthetized and its left cochlea was exposed. Tones from a loudspeaker were delivered to the ear via a tube fitted to the left ear canal. The level of the tones was calibrated in the ear canal at the beginning of each experiment. Basal scala tympani pressure measurements were made by inserting a pressure sensor through the round window opening after removing the covering membrane. Scala vestibuli and turn-one scala tympani measurements were made through small holes hand-drilled in the cochlear bone. In basal experiments it was possible to see the basilar membrane in order to position the scala tympani sensor. In turn-one experiments it was positioned by using anatomical landmarks and referring to widely opened excised cochleae. It was not practical to systematically check the precision of positioning in each experiment. However, the grouped data indicate that incorrectly positioning the sensor towards the spiral ligament caused substantial damage, and that incorrectly positioning the sensor over the spiral lamina caused greatly diminished pressure gradients. The distance between the basilar membrane and the sensor was determined by touching the former with the latter, which produced a characteristically noisy signal.

Stimulus generation and recording was performed with a Tucker Davis Technologies DA/AD system. With typical signal averaging times of 3 s, sound pressure above the level of 60–70 dB SPL (20–60 mPa) could be reliably measured.

As a gauge of cochlear health, an electrode at the round window measured the CAP response of the auditory nerve to tones. The CAP threshold is the minimum sound level required to elicit a reliable neural response. Initial thresholds in the turn one experiment were ≤30 dB SPL at 15 and 20 kHz, and 50 dB SPL at 25 kHz. Close to the time of measurements, these thresholds were 40, 40, and 50–60 dB SPL. Initial thresholds in the basal experiment were ≤60 dB SPL at 30 kHz, and 80 dB SPL at 40 kHz. Close to the time of measurements, they were 60 and >80 dB SPL. At the frequencies of interest, the initial CAP thresholds in the turn one experiment were in keeping with those of Müller<sup>9</sup>, those in the basal experiment were elevated somewhat. The degree of nonlinearity observed in the scala tympani pressures was consistent with the health of the cochlea as indicated by the CAP threshold—the basal experiment was nearly linear, and the nonlinearity in the turn-one experiment was strong, but not among the strongest in the literature<sup>9</sup>.

Received 1 June; accepted 4 October 1999.

1. von Bekesy, G. *Experiments in Hearing* (McGraw Hill, New York, 1960).
2. Olson, E. S. Observing middle and inner ear mechanics with novel intracochlear pressure sensors. *J. Acoust. Soc. Am.* **103**, 3445–3463 (1998).
3. Brownell, W. E., Bader, C. R., Betrand, D. & de Ribaupierre, Y. Evoked mechanical responses of isolated cochlear outer hair cells. *Science* **227**, 195–196 (1985).
4. Liberman, M. C. & Dodds, L. W. Single neuron labeling and chronic cochlear pathology. III. Stereocilia damage and alterations of threshold tuning curves. *Hear. Res.* **16**, 55–74 (1984).
5. Spoendlin, H. Innervation densities of the cochlea. *Acta Otolaryngol. (Stockh.)* **73**, 235–248 (1972).
6. Müller, M. The cochlear place-frequency map of the adult and developing mongolian gerbil. *Hear. Res.* **94**, 148–156 (1996).
7. Dancer, A. & Franke, R. Intracochlear sound pressure measurements in guinea pigs. *Hear. Res.* **2**, 191–205 (1980).
8. Rhode, W. S. Observations of the vibration of the basilar membrane in squirrel monkeys using the Mossbauer Technique. *J. Acoust. Soc. Am.* **49**, 1218–1231 (1971).
9. Ruggero, M., Rich, N. C., Recio, A., Narayan, S. S. & Robles, L. Basilar membrane responses to tones at the base of the chinchilla cochlea. *J. Acoust. Soc. Am.* **101**, 2151–2163 (1997).
10. Lighthill, J. Energy flow in the cochlea. *J. Fluid Mech.* **106**, 149–213 (1981).
11. Sellick, P. M., Yates, G. K. & Patuzzi, R. The influence of Mossbauer source size and position on phase and amplitude measurements of the guinea pig basilar membrane. *Hear. Res.* **10**, 101–108 (1983).
12. Xue, S., Mountain, D. C. & Hubbard, A. E. Electrically evoked basilar membrane motion. *J. Acoust. Soc. Am.* **97**, 3030–3041 (1995).
13. Cooper, N. P. & Rhode, W. S. Basilar membrane mechanics in the hook region of cat and guinea-pig

cochlea: Sharp tuning and nonlinearity in the absence of baseline position shifts. *Hear. Res.* **63**, 163–190 (1992).

14. de Boer, E. Auditory physics. Physical principles in hearing theory. II. *Phys. Rep.* **105**, 141–226 (1984).
15. Steele, C. R. & Taber, L. A. Comparison of WKB calculations and experimental results for three-dimensional cochlear models. *J. Acoust. Soc. Am.* **65**, 1007–1018 (1979).
16. Plassman, W., Peetz, W. & Schmidt, M. The cochlea in gerbilline rodents. *Brain Behav. Evol.* **30**, 82–101 (1987).

**Acknowledgements**

I thank H. Nakajima, E. de Boer, L. Sohn, N. Cooper, S. Staggs, R. Brawer, R. Austin and L. Page Jr. This work was supported by the National Institute on Deafness and Other Communication Disorders.

Correspondence and requests for materials should be addressed to E.O. (e-mail: eolson@princeton.edu).

**Stable propagation of synchronous spiking in cortical neural networks**

Markus Diesmann\*, Marc-Oliver Gewaltig\* & Ad Aertsen

Department of Neurobiology and Biophysics, Institute of Biology III, Albert-Ludwigs-University, Schänzlestraße 1, D-79104 Freiburg, Germany

The classical view of neural coding has emphasized the importance of information carried by the rate at which neurons discharge action potentials. More recent proposals that information may be carried by precise spike timing<sup>1–5</sup> have been challenged by the assumption that these neurons operate in a noisy fashion—presumably reflecting fluctuations in synaptic input<sup>6</sup>—and, thus, incapable of transmitting signals with millisecond fidelity. Here we show that precisely synchronized action potentials can propagate within a model of cortical network activity that recapitulates many of the features of biological systems. An attractor, yielding a stable spiking precision in the (sub)millisecond range, governs the dynamics of synchronization. Our results indicate that a combinatorial neural code, based on rapid associations of groups of neurons co-ordinating their activity at the single spike level, is possible within a cortical-like network.

Evidence is accumulating that cortical neurons *in vivo* are capable of producing action potentials with high temporal accuracy. In recordings of multiple single-neuron activity in behaving monkeys, precisely timed action potentials have been systematically related to stimuli and behavioural events, indicating that these instances of precise spike timing play a functional role<sup>1–3</sup>. Independent evidence for precise spike timing in cortical neurons came from intracellular recordings *in vitro*<sup>4,5</sup>. But can an instance of synchronous spiking, once it has occurred, be successfully propagated by subsequent groups of cortical neurons? Under which input conditions can a group of cortical neurons engage in precisely coordinated spike timing, and are such conditions feasible in the cortical network? How can we clarify and quantify the notions of 'well timed' and 'reliable', which gained such a prominent role in the on-going debate on temporal coding in the brain?<sup>7–10</sup> Clearly, these questions must be resolved to determine whether cortical computation on the basis of precise spike timing is possible. Preliminary results have been presented in abstract form<sup>11,12</sup>.

To address these questions, we have studied the fine-grained temporal response properties of the 'integrate-and-fire' neuron, a widely used class of model neurons capturing essential properties of

\* Present addresses: Department of Nonlinear Dynamics, Max-Planck-Institut für Stömungsforschung, Göttingen, Germany (M.D.); Future Technology Research, Honda R&D Europe, Offenbach, Germany (M.-O.G.)

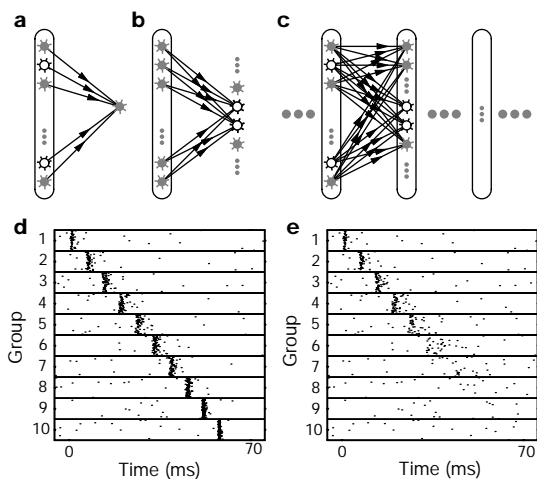


**Figure 1** Propagation of synchronous spiking in cortical networks. Effect **(a)** and generation **(b)** of tight spike correlation by convergence of synchronous shared input onto target neurons (simultaneously recorded neurons are highlighted by black circles). **c**, Combination of **a** and **b** (no intragroup connections) generates synchronous spike volley. Propagation across neuron groups by repeating the arrangement ('synfire chain'<sup>17</sup>) can be stable **(d)** or unstable **(e)**. **d, e**, Raster displays of propagating spike volley along fully connected synfire chain. Panels show the spikes in 10 successive groups of 100 neurons each (synaptic delays arbitrarily set to 5 ms). Initial spike volley (not shown) was fully synchronized ( $\sigma = 0$  ms), containing  $a = 50$  **(d)** or  $a = 48$  **(e)** spikes; background activity identical in both cases.

the firing behaviour of cortical neurons<sup>13,14</sup>. We focused on spike responses to transient membrane-potential excursions, implied by the physiological findings<sup>1-5</sup>. As a rule, such transients are explained by convergent inputs from simultaneously spiking neurons onto a target neuron (Fig. 1a). These transients, in turn, result in well timed response spikes in target neurons. Neurons that share a large enough pool of simultaneously discharging input cells tend to align their action potentials<sup>15</sup> (Fig. 1b). By repeating this arrangement, a group of neurons can reproduce its synchronous input activity and act as the source of synchronous shared input to the following group (Fig. 1c). This idea of connecting groups of neurons into feed-forward arrangements<sup>16</sup> was formalized by Abeles in the 'synfire chain'<sup>17</sup>. The degree of temporal accuracy of spike times among the group's members determines whether subsequent groups can reproduce (or even improve) this accuracy (Fig. 1d), or whether synchronous excitation disperses and eventually dies out (Fig. 1e). Thus, in the context of cortical network function, the timing precision of a neuron's action potentials is measured *vis-à-vis* the timing of those of its companion neurons; the quality of timing is judged on the effect the group's activity has in the network, that is, whether synchronous spiking is sustained or whether it dies out.

Existing measures of short-term dynamics in neural transmission focus on two extreme cases of input activity: full synchrony and random arrival of spikes<sup>18-20</sup>. Intermediate cases with limited degree of temporal dispersion are generally not addressed. 'Pulse packets'<sup>21,12</sup> were introduced to overcome this restriction and to quantify the degree of synchrony in a propagating spike volley. A pulse packet characterizes a spike volley by two parameters: activity,  $a$ , and temporal dispersion,  $\sigma$ . Activity is defined as the number of spikes in the volley; their temporal dispersion is measured by the standard deviation of the underlying pulse density (Fig. 2a). Thus, in simulations we measured the response of a cortical model neuron (see Methods) to different pulse-packet inputs in the presence of background activity (Fig. 2b). The neuronal transmission function for transient input activity is defined by the transformation of the input pair ( $a_{in}, \sigma_{in}$ ) into the output pair ( $\alpha, \sigma_{out}$ ), where  $\alpha$  is the single neuron response probability. The firing probability curves (Fig. 2c)

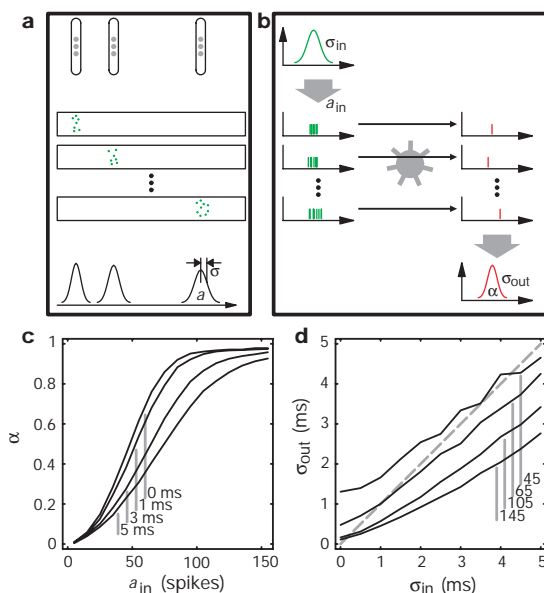


**Figure 2** Neural transmission function for pulse-packet input. **a**, Pulse-packet representation of propagating spike volley. **b**, Cortical model neuron, stimulated with pulse packets by repeatedly drawing  $a_{in}$  spike times from Gaussian pulse density with standard deviation  $\sigma_{in}$  (green). Pulse packets were embedded in random spikes, mimicking background activity. The neuron responded with one spike at most, its timing varying trial by trial. The temporal distribution was measured by trial averaging (red). Net area under curve, spike probability  $\alpha$ ; standard deviation, response jitter  $\sigma_{out}$ . **c**, Spike probability versus input spike number for different degrees of input synchrony. **d**, Temporal accuracy of spike response versus input synchrony for different input spike numbers. The diagonal (dashed grey line) marks points with equal temporal precision of input and response.

resemble the well known sigmoid activation function, the slope is determined by the degree of input synchrony (the saturation slightly below 1 reflects the chance that the neuron was refractory on stimulus arrival). As expected, the spread of the response distribution (Fig. 2d) increases with the input spread; however, the slope is less than 1, hence output spread increases more slowly than input spread. In addition, the curves show an offset; even for fully synchronized volleys ( $\sigma_{in} = 0$  ms), some residual jitter of the response spike remains, reflecting the influence of background activity. Hence, each dispersion curve crosses the diagonal at some critical value of input synchrony. Up to this intersection, the neuron's response is less precise than the input, that is, synchronous input is desynchronized. Beyond the intersection, however, the neuron's spike response is more precise than the input, that is, the neuron exhibits a synchronizing behaviour. Duplication of the experiment with identical input pulse-packet realizations across trials yielded essentially the same results, confirming that trial-by-trial response variability is due to fluctuations in background activity<sup>21</sup>.

We used this neuronal transmission function to test whether the cortical network is capable of sustaining synchronous spiking activity. As each neuron responds to an incoming pulse packet with at most one spike, stable propagation of synchronous spike volleys inevitably requires the activation of successive, large enough groups of neurons (Fig. 1c). For a group of identical independent neurons, the distribution of response spikes to an input pulse packet is identical to the response distribution for a single neuron (Fig. 2). Thus, the spread of the group's response equals the single neuron's response dispersion  $\sigma_{out}$  (Fig. 2d). The expected number of response spikes  $a_{out}$  in a group equals  $\alpha$  (Fig. 2c) multiplied by the group size  $w$ . Figure 3a, b (grey curves) shows the input-output relation for a group of  $w = 100$  neurons. Assuming that the group's response to a

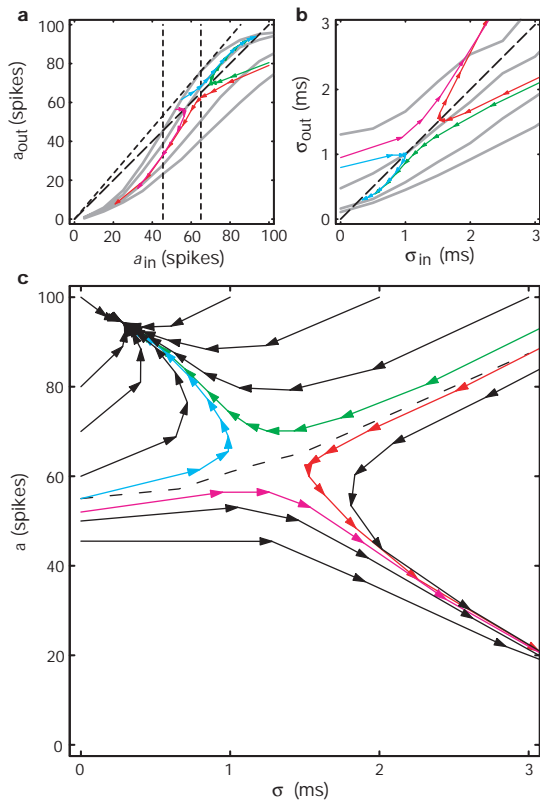


**Figure 3** State-space analysis of propagating spike synchrony. **a, b**, Grey curves, transmission function for pulse-packet input for a group of  $w = 100$  neurons. Coloured curves, evolution of synchronous spike volley along a chain of such groups (Fig. 1c) for different input configurations. Arrows, group to group transformation. Two cases of stable propagation are shown, one starting with few, fully synchronized spikes (blue; see Fig. 1d), the other with many, weakly synchronized spikes (green), and two unstable cases where synchronous activity rapidly dies out (red, purple; see Fig. 1e). **c**, State space portrait of dynamic variables  $a$  and  $\sigma$ . Coloured trajectories portray the four cases in **a, b**. The stable (upper) and unstable (lower) regimes are separated by the separatrix (dashed line).

spike volley is adequately described by  $a$  and  $\sigma$  (see Methods: Fluctuations), we can capture the evolution of synchronous spiking activity by repeatedly applying the  $(a, \sigma)$ -transformation while moving from one group to the next (Fig. 3a, b, coloured curves). Thus, the evolution of synchronous activity on its course through the network is described by a trajectory in the 2-dimensional state space, spanned by  $a$  and  $\sigma$  (Fig. 3c).

The state-space portrait exhibits two fixpoints: an attractor ( $a = 95$ ,  $\sigma = 0.5$  ms), and a saddle point ( $a = 65$ ,  $\sigma = 1.2$  ms). A separatrix (dashed line) running through the saddle point divides

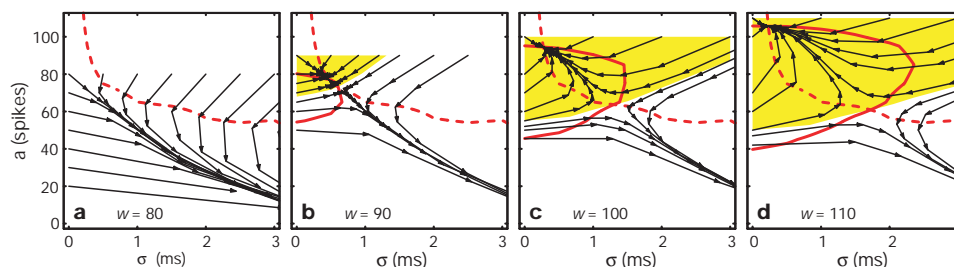


**Figure 4** Dependence of the spike synchrony state space on the size of the neuron groups. **a–d**, State-space portraits of propagating spike synchrony for four different group sizes  $w$ , increasing from  $w = 80$  (**a**) in steps of 10 up to  $w = 110$  (**d**). In each

the state space into two regimes. In the basin of attraction, all trajectories converge into the attractor. A spike volley starting anywhere inside this regime rapidly (that is, after only few stages) reaches a stable configuration ( $\sim 95$  spikes) with submillisecond dispersion. Volleys starting outside the stable regime decay after only few stages; too weak or too dispersed activity rapidly dies out. Note that neither the relationship between input and output activity (Fig. 3a) nor that between input and output jitter<sup>10</sup> (Fig. 3b) alone determines whether synchronous activity survives. The nonmonotonic evolution of these variables along a trajectory (Fig. 3c, coloured curves) demonstrates this fact. An initial increase in temporal spread may still support stable propagation, provided that the number of spikes in the volley is large enough (blue). If, however, this number is too small, the volley dies out, in spite of its initial increase (purple). Conversely, synchronous activity may still vanish with an initial decrease in dispersion (red), unless the volley is large enough (green). Thus, the system dynamics are governed by the interaction of the two state variables.

Evidently, the number of neurons per group influences the evolution of the activity (see Fig. 3a). The analysis in Fig. 3 was made using the group size  $w = 100$ . To determine how many simultaneously firing neurons are needed to guarantee that synchronous activity survives in the network, we examined how the structure of the state space depends on the groups size (Fig. 4). For increasing numbers of neurons per group, the two fixpoints move apart, thereby increasing the basin of attraction (yellow). The regime over which synchronous spiking survives in the network increases accordingly. By contrast, for decreasing groups size, the two fixpoints approach each other until, at some critical value (here  $w = 89$ ), they merge into a single saddle node. Below this critical value, no fixpoint exists and, hence, all trajectories lead to extinction (Fig. 4a). Thus, a minimum of some 90 neurons per group is needed to maintain precise spike synchrony. This lower bound is essentially determined by the ratio of the distance from mean membrane potential to spike threshold and the postsynaptic potential (PSP) amplitude; stronger intergroup synapses reduce this number (see Methods: Fluctuations).

Our results show that for a wide range of amplitudes and dispersions of spike input distributions, the response of successively activated groups of cortical neurons is governed by an attractor, which describes a stationary configuration of activity in  $(a, \sigma)$  space. However, unlike the Hopfield attractor<sup>22</sup>, this attractor describes a dynamic activity configuration in neuron space, that is, different neuron groups, one after the other, contribute single spikes to the propagating synchronous wave. The basin of attraction guarantees robustness of the propagating synchrony against perturbations exceeding the response variability accounted for by the transmission function (Fig. 2). Thus, temporal dispersion due to differences in axonal or dendritic delays, fluctuations in synaptic transfer properties or correlated background fluctuations will not destroy the synchronous transmission, as long as they do not push the network outside the basin of attraction.

panel, the continuous red line indicates the  $a$ -isocline, the red dashed line indicates the  $\sigma$ -isocline (see Methods: Isoclines). The intersections of the two isoclines define the fixpoints. The basin of attraction is indicated in yellow.

In the stable state, essentially all response spikes in a volley fall within  $\pm 1$  ms. This temporal precision is consistent with the accuracy of observed spike patterns in cortical recordings<sup>1–3</sup>. Thus, in contrast to other studies using this neuron model<sup>7,8</sup>, we conclude that precise synchronous firing of cortical neurons is indeed feasible, in spite of the membrane time constant of 10 ms or more (see Methods: Membrane time constant). The notion of pulse packets yields a natural solution to the question of whether the cortical neuron acts as ‘integrator’ or ‘coincidence detector’—a question raised many years ago<sup>18</sup> and revived recently<sup>7–10</sup>—by embedding these two conceptions in a single framework. The temporal structure of the input determines which of the two aspects is emphasized.

For each neuron in our network model, the synapses delivering activity from the preceding group and the synapses delivering background activity were set at equal strength. Our findings show that stable transmission of synchronous spiking does not require dedicated strong synapses, provided enough neurons can be recruited in successive groups. Each neuron in a group contributes a single spike to the passing volley. Once the neuron recovers from refractoriness, it is ready to engage in another group. Thus, each neuron may participate—spike by spike, not limited by a specific arrangement of synaptic weights—in multiple volleys with different neuron compositions, provided its engagements differ by more than the refractory period. Hence, the network only needs to be locally feed forward. Several such volleys may propagate through the network simultaneously, allowing multiple synchronous processes to coexist while maintaining their identities<sup>23,24</sup>. Their degree of temporal coupling may differ, depending on overlap (numbers and arrangement of shared neurons and inputs)<sup>23,25</sup>. This scheme indicates that a combinatorial neural code, based on the continual reconfiguration of the cortical network into short-lived functional groups depending on the immediate computational demands, is compatible with biological constraints. □

## Methods

### Model neuron

Simulations were performed using a leaky-integrator with voltage-threshold model<sup>13,14</sup>, with physiological and anatomical parameters taken from experimental literature. The model neuron (membrane time constant 10 ms, resting potential  $-70$  mV, spike threshold  $-55$  mV, absolute refractoriness 1 ms, relative refractoriness ( $\tau \approx 15$  ms) modelled by K-conductances) was supplied with synaptic noise input, reflecting on-going activity in the cortical network (20,000 synapses: 88% excitatory, 12% inhibitory)<sup>26</sup>. Postsynaptic currents (PSCs) were modelled by an  $\alpha$ -function to yield realistic PSPs (peak amplitude 0.14 mV, time-to-peak 1.7 ms, half-width 8.5 ms)<sup>27</sup>. Identical values were used for inter-group and background connections; excitatory and inhibitory PSPs only differed in sign. Background firing rates (excitatory, 2 Hz; inhibitory, 12.5 Hz; all uncorrelated stationary Poisson) were chosen to yield an output rate of 2 Hz. At this consistency condition, output statistics were approximately Poisson, membrane potential shot noise (mean 8.25 mV, s.d. 2.85 mV) was close to ‘balanced’ excitation/inhibition<sup>28</sup>. It can be shown that details of the construction of background fluctuations are not essential. Simulations were performed in 0.1 ms time steps using the simulation tool SYNOD<sup>29</sup>.

### Threshold packet

The  $(a_{in}, a_{out})$  curves (grey) in Fig. 3a cross the diagonal (dashed) in two points. Here, the number of output spikes equals the number of input spikes. The lowest intersection (at the left-most vertical line) occurs with the curve for fully synchronized input ( $\sigma_{in} = 0$ ), defining a lower boundary on the size of the threshold packet, that is, the minimum input spike number needed to reach the attractor. Smaller packets cannot survive, since for other curves, the output spike number is even smaller. Decreasing the group’s size rotates the diagonal relative to the  $(a_{in}, a_{out})$  curves counterclockwise around the origin; the intersection points approach each other and the threshold packet size increases. Thus, for decreasing  $w$ , more curves fall below the diagonal until even the curve for fully synchronized input only touches (short-dashed oblique line intersection with right-most vertical line). For smaller groups, all curves run below the diagonal; the attractor vanished, and stable propagation of synchronous spiking is no longer possible.

### Isoclines

The  $a$ -isocline is the collection of states for which the spike number in a volley does not change from stage to stage, irrespective of  $\sigma$  (Fig. 4b–d, solid red curves). The  $\sigma$ -isocline contains all states maintaining temporal spread, irrespective of  $a$  (Fig. 4a–d, dashed red curves). Thus, the isoclines are the loci of horizontal/vertical flow. The fixpoints (neither a

nor  $\sigma$  changes) are the intersections of the isoclines. The  $\sigma$ -isocline is independent of  $w$  (Fig. 3b). The spike number, however, is proportional to  $w$  (Fig. 3a). Hence, with decreasing  $w$  (Fig. 4d to 4a), the  $a$ -isocline shrinks and moves left until it ceases to exist. Thus, the group’s size  $w$  acts as bifurcation parameter, controlling the existence and separation of fixpoints.

### Fluctuations

As confirmed by network simulations (M.-O.G., manuscript in preparation), the state-space portrait derived here describes the evolution of synchronous activity in the mean, that is, by subsequent values of the expectation  $(a, \sigma)$  across trials with different background activity realizations. Around each point of a trajectory, these realizations form a distribution with width determined by  $a$ ,  $\sigma$ ,  $w$  and intergroup connectivity. This width becomes more important near the separatrix because of the increased probability—even for trajectories stable in the mean—that individual realizations leave the basin of attraction (and vice versa). Upscaling the synaptic weights by a factor up to 10 while downscaling the groups size accordingly does not alter the structure of the state space, except close to the separatrix where the probability to leave the basin of attraction increases. The contribution of individual input spikes grows; consequently, fluctuations in membrane-potential response to pulse-packet realizations with identical parameters and, hence, trial-by-trial variability, increases.

### Background activity

Background activity in different neurons was considered independent, stationary Poisson. However, on-going cortical activity is known to exhibit coherent spatio-temporal structure<sup>30</sup>. Hence, anatomically nearby neurons within a group tend to be excited (inhibited) together. This affects the pulse-packet properties needed to make these neurons fire simultaneously. The impact of such coherence in background activity is currently being studied.

### Membrane time constant

The temporal precision of spike response is not constrained by membrane time constant itself; the limiting factor is the up slope of the excitatory PSP. The larger this slope, the faster the membrane-potential response to a pulse packet traverses the threshold region<sup>17</sup>. This reduces the chance of interference with background fluctuations, which degrade response spike precision. The membrane time constant does, however, limit transmission of synchronous spikes in the opposite way. It determines the integration time window of the receiving neuron, limiting the extent over which a spike volley is ‘seen’ as a single packet, rather than as individual spikes. For a too-small membrane time constant, PSPs no longer overlap and cannot add up to threshold. Reliable transmission of incompletely synchronized spike volleys, therefore, requires a minimal (rather than maximal) membrane time constant, in the order of the volley duration.

Received 17 June; accepted 23 August 1999.

1. Abeles, M., Bergman, H., Margalit, E. & Vaadia, E. Spatiotemporal firing patterns in the frontal cortex of behaving monkeys. *J. Neurophysiol.* **70**, 1629–1638 (1993).
2. Prut, Y. et al. Spatiotemporal structure of cortical activity: Properties and behavioral relevance. *J. Neurophysiol.* **79**, 2857–2874 (1998).
3. Riehle, A., Grün, S., Diesmann, M. & Aertsen, A. Spike synchronization and rate modulation differentially involved in motor cortical function. *Science* **278**, 1950–1953 (1997).
4. Mainen, Z. F. & Sejnowski, T. J. Reliability of spike timing in neocortical neurons. *Science* **268**, 1503–1506 (1995).
5. Nowak, L. G., Sanchez-Vives, M. V. & McCormick, D. A. Influence of low and high frequency inputs on spike timing in visual cortical neurons. *Cereb. Cortex* **7**, 487–501 (1997).
6. Calvin, W. H. & Stevens, C. F. Synaptic noise and other sources of randomness in motoneuron interspike intervals. *J. Neurophysiol.* **31**, 574–587 (1968).
7. Shadlen, M. N. & Newsome, W. T. Noise, neural codes and cortical organization. *Curr. Opin. Neurobiol.* **4**, 569–579 (1994).
8. Shadlen, M. N. & Newsome, W. T. The variable discharge of cortical neurons: Implications for connectivity, computation, and information coding. *J. Neurosci.* **18**, 3870–3896 (1998).
9. König, P., Engel, A. K. & Singer, W. Integrator or coincidence detector? The role of the cortical neuron revisited. *Trends Neurosci.* **19**, 130–137 (1996).
10. Marsalek, P., Koch, C. & Maunsell, J. On the relationship between synaptic input and spike output jitter in individual neurons. *Proc. Natl Acad. Sci. USA* **94**, 735–740 (1997).
11. Diesmann, M., Gewaltig, M.-O. & Aertsen, A. in *Computational Neuroscience—Trends in Research 1995* (ed. Bower, J.) 59–64 (Academic, San Diego, 1996).
12. Diesmann, M., Gewaltig, M.-O. & Aertsen, A. in *From Membrane to Mind* (eds Elsner, N. & Wässle, H.) 62 (Thieme, Stuttgart, 1997).
13. Gerstein, G. L. & Mandelbrot, B. Random walk models for the spike activity of a single neuron. *Biophys. J.* **4**, 41–68 (1964).
14. Tuckwell, H. C. *Introduction to Theoretical Neurobiology* (Cambridge Univ. Press, Cambridge, 1988).
15. Perkel, D. H., Gerstein, G. L. & Moore, G. P. Neuronal spike trains and stochastic point processes. II. Simultaneous spike trains. *Biophys. J.* **7**, 419–440 (1967).
16. Griffith, J. S. On the stability of brain-like structures. *Biophys. J.* **3**, 299–308 (1963).
17. Abeles, M. *Corticonics* (Cambridge Univ. Press, Cambridge, 1991).
18. Abeles, M. Role of cortical neuron: integrator or coincidence detector? *Isr. J. Med. Sci.* **18**, 83–92 (1982).
19. Bernander, O., Koch, C. & Usher, M. The effect of synchronized inputs at the single neuron level. *Neural Comp.* **6**, 622–641 (1994).
20. Murthy, V. N. & Fetz, E. E. Effects of input synchrony on the firing rate of a three-conductance cortical neuron model. *Neural Comp.* **6**, 1111–1126 (1994).
21. Arieli, A., Sterkin, A., Grinvald, A. & Aertsen, A. Dynamics of ongoing activity: explanation of the large variability in evoked cortical responses. *Science* **273**, 1868–1871 (1996).

22. Hopfield, J. J. Neural networks and physical systems with emergent collective computational abilities. *Proc. Natl. Acad. Sci. USA* **79**, 2554–2558 (1982).
23. Bienenstock, E. A model of neocortex. *Network* **6**, 179–224 (1995).
24. Herrmann, M., Hertz, J. A. & Prügel-Bennett, A. Analysis of synfire chains. *Network* **6**, 403–414 (1995).
25. Arnoldi, H.-M. R. & Brauer, W. Synchronization without oscillatory neurons. *Biol. Cybern.* **74**, 209–223 (1996).
26. Braitenberg, V. & Schüz, A. *Anatomy of the Cortex* (Springer, Berlin, 1991).
27. Fetz, E., Toyama, K. & Smith, W. in *Cerebral Cortex* Vol. 9 (eds Peters, A. & Jones, E. G.) 1–47 (Plenum, New York, 1991).
28. van Vreeswijk, C. & Sompolinsky, H. Chaos in neuronal networks with balanced excitatory and inhibitory activity. *Science* **274**, 1724–1726 (1996).
29. Diesmann, M., Gewaltig, M.-O. & Aertsen, A. *SYNOD: An Environment for Neural Systems Simulations* Technical report GC-AA/95-3 (The Weizmann Institute of Science, Rehovot, Israel, 1995). (<http://www.synod.uni-freiburg.de>).
30. Arieli, A., Shoham, D., Hildesheim, R. & Grinvald, A. Coherent spatiotemporal patterns of ongoing activity revealed by real-time optical imaging coupled with single-unit recording in the cat visual cortex. *J. Neurophysiol.* **73**, 2072–2093 (1995).

**Acknowledgements**

We thank M. Abeles, E. Bienenstock, S. Grün, I. Nelken, A. Riehle, S. Rotter and C. von der Malsburg for their constructive comments. Supported in part by grants for the Deutsche Forschungsgemeinschaft, the German–Israeli Foundation for Scientific Research and Development, and Human Frontier Science Program.

Correspondence and requests for materials should be addressed to A.A. (e-mail: aertsen@biologie.uni-freiburg.de).

.....

## Membrane-anchored aspartyl protease with Alzheimer’s disease $\beta$ -secretase activity

Riqiang Yan\*†, Michael J. Bienkowski†‡, Mary E. Shuck‡, Huiyi Miao\*, Monica C. Tory‡, Adele M. Pauley§, John R. Brashler||, Nancy C. Stratman§, W. Rodney Mathews¶, Allen E. Buhll||, Donald B. Carter§, Alfredo G. Tomasselli#, Luis A. Parodi‡, Robert L. Heinrikson# & Mark E. Gurney§

\* Cell & Molecular Biology, † Genomics, # Protein Sciences, || Pharmacology, ¶ Structural, Analytical & Medicinal Chemistry and § Neurobiology, Pharmacia & Upjohn, Inc., 301 Henrietta Street, Kalamazoo, MI 49007, USA  
 ‡ Bioinformatics, Pharmacia & Upjohn, Inc., Lindhagensgatan 133, S-11287 Stockholm, Sweden  
 † These authors contributed equally to this work

.....

**Mutations in the gene encoding the amyloid protein precursor (APP) cause autosomal dominant Alzheimer’s disease<sup>1–3</sup>. Cleavage of APP by unidentified proteases, referred to as  $\beta$ - and  $\gamma$ -secretases<sup>4–7</sup>, generates the amyloid  $\beta$ -peptide, the main component of the amyloid plaques found in Alzheimer’s disease patients<sup>8</sup>. The disease-causing mutations flank the protease cleavage sites in APP and facilitate its cleavage. Here we identify a new membrane-bound aspartyl protease (Asp2) with  $\beta$ -secretase activity. The Asp2 gene is expressed widely in brain and other tissues. Decreasing the expression of Asp2 in cells reduces amyloid  $\beta$ -peptide production and blocks the accumulation of the carboxy-terminal APP fragment that is created by  $\beta$ -secretase cleavage. Solubilized Asp2 protein cleaves a synthetic APP peptide substrate at the  $\beta$ -secretase site, and the rate of cleavage is increased tenfold by a mutation associated with early-onset Alzheimer’s disease in Sweden<sup>3</sup>. Thus, Asp2 is a new protein target for drugs that are designed to block the production of amyloid  $\beta$ -peptide and the consequent formation of amyloid plaque in Alzheimer’s disease.**

Visual inspection suggests that the  $\beta$ - and  $\gamma$ -secretase cleavage sites in APP might be substrates for cleavage by aspartyl proteases,

and indeed, cathepsin D cleaves synthetic  $\beta$ -secretase substrates<sup>9</sup>. This cleavage is facilitated by the KM  $\rightarrow$  NL mutation, referred to as the ‘Swedish’ mutation, found in patients with early-onset Alzheimer’s disease<sup>10</sup>; however, APP processing to amyloid  $\beta$  (A $\beta$ ) peptides occurs normally in hippocampal neurons cultured from cathepsin-D-null mice<sup>11</sup>. Nevertheless, it seemed plausible that the APP  $\beta$ - or  $\gamma$ -secretases could be as yet uncharacterized aspartyl proteases; therefore, we searched for new human enzymes of this mechanistic set. Sequencing of the *Caenorhabditis elegans* genome was nearing completion, which offered the possibility of enumerating the complete set of aspartyl proteases encoded in a simple metazoan genome, and using these as a bridge to human sequence databases.

Simple AWK scripts scanning for the D(S/T)G active-site motif, PROSITE and hidden Markov models were used to search the WormPep database of predicted *C. elegans* proteins. This revealed at least 10 candidate aspartyl proteases. Seven of these ten were found on a single chromosome, chromosome V (*F21F8.3*, *F21F8.4*, *F21F8.7*, *Y39B6B.G*, *Y39B6B.J*, *Y39B6B.H* and *T18H9.2*), and three each of these were found in the same cosmid clones (*F21F8* and *Y39B6B*), suggesting that they represent a recently evolved family of proteins that arose by ancestral gene duplication. Other homologous predicted genes were found in the same cluster (*F21F8.2*, *F21F8.6* and *Y39B6B.I*); however, these contain only a single DTG or DSG motif. Additional predicted aspartyl protease genes were found on chromosomes IV (*C11D2.2*) and X (*R12H7.2* and *H22K11.1*). Searches of vertebrate expressed sequence tag (EST) databases with the 10 *C. elegans* sequences identified 7 known and 4 new candidate aspartyl proteases. The new human sequences were numbered in order of their discovery (Asp1–4). *R12H7.2* and *H22K11.1* appear to be *C. elegans* homologues of cathepsin D. Most of the chromosome V aspartyl proteases had no clear vertebrate orthologues; however, one of these (*T18H9.2*) bridged to two unusual sequences (Asp1 and Asp2) which contained the less common DSG motif in the second active site. In turn, *C11D2.2* identified two additional sequences (Asp3 and Asp4) which have since been reported in the literature as napsins A and B<sup>12</sup>.

The two predicted aspartyl protease sequences identified by *T18H9.2* were of greatest interest. Completion of their sequences by a combination of EST sequencing, 5’ rapid amplification of complementary DNA ends by the polymerase chain reaction, and library screening showed that both Asp1 and Asp2 had an unusual C-terminal extension containing a single predicted transmembrane domain (Fig. 1). Asp1 maps to human chromosome 21q22 within the Down’s syndrome critical region, and Asp2 to chromosome 11q23–24. Northern hybridization to human tissue blots showed widespread expression of both Asp1 and Asp2. Both are expressed at the highest levels in pancreas. Asp2 is also expressed at high levels in brain, whereas Asp1 is expressed in brain at somewhat lower levels. *In situ* hybridization showed expression of Asp2 primarily in acinar cells of the exocrine pancreas, whereas faint hybridization was seen over neurons in hippocampus; however, we identified two Asp2 EST in a human astrocyte cDNA library indicating that Asp2 may be expressed in both neurons and glial cells. Transcripts for both Asp1 and Asp2 were expressed in human embryonic kidney 293 cells, human IMR-32 neuroblastoma cells and mouse Neuro-2a neuroblastoma cells, three commonly used cellular models of APP processing.

We used a panel of antisense oligomers to test the involvement of each of the four predicted aspartyl proteases in APP processing by a stable clone of HEK293 cells that had been engineered to process APP to A $\beta$  peptides at high levels. These cells were transformed with a modified human APP695 cDNA containing the Swedish KM  $\rightarrow$  NL mutation to which two lysine residues had been added to the C terminus (HEK/APP-Sw-KK cells). The KK motif greatly increases the processing and release of A $\beta$  peptides but does not influence the ratio of A $\beta$ 42/(A $\beta$ 42 + A $\beta$ 40), nor alter the effect of